ACS APPLIED MATERIALS & INTERFACES

Letter

www.acsami.org

Glycine Crystallization in Solution by CW Laser-Induced Microbubble on Gold Thin Film Surface

Takayuki Uwada,*[,†,‡] Sho Fujii,[§] Teruki Sugiyama,[‡,⊥] Anwar Usman,[†] Atsushi Miura,[†] Hiroshi Masuhara,*[,†,‡] Katsuhiko Kanaizuka,[§] and Masa-aki Haga[§]

[†]Department of Applied Chemistry and Institute of Molecular Science, National Chiao Tung University, Hsinchu 30010, Taiwan

[‡]Graduate School of Materials Science, Nara Institute of Science and Technology, Ikoma, Nara 630-0192, Japan

[§]Department of Applied Chemistry, Faculty of Science and Engineering,Chuo University, Bunkyo-ku, Tokyo112-8551, Japan

[⊥]Instrument Technology Research Center, National Applied Research Laboratories, Hsinchu 30076, Taiwan

Supporting Information

ABSTRACT: We have developed a novel laser-induced crystallization method utilizing local heat-induced bubble/water interface. Continuous laser beam of 1064 nm is focused on a gold nanoparticles thin film surface covered with glycine supersaturated aqueous solution. Light absorption of the film due to localized plasmon resonance caused local heating at the focal position and produced a single thermal vapor microbubble, which generated thermal gradient followed by convection flow around the bubble and eventually induced glycine crystallization and growth. The crystallization mechanism is discussed by considering gathering and accumulating molecules around the bubble/water interface assisted by convection flow and temperature jump.

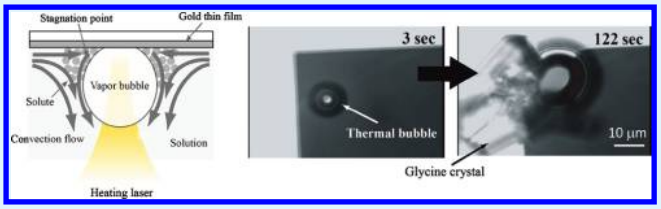

KEYWORDS: *laser-heating, vapor bubble, gold thin film, glycine, crystallization, convection flow*

Light-induced crystallization of organic and biological molecules has attracted much attention from the viewpoint of a fundamental interest in light-matter interactions and in the fields of crystal science and engineering. Until now, several groups, including our group, have succeeded in developing laser-induced crystallization techniques,[1−15] which can be classified into two groups, photophysical crystallization and photochemical one. The former employs optical Kerr effect,[1−4] laser trapping,[5−8] or transient pressure,[9,11−13] i.e., laser-oriented physical phenomena for molecular accumulation and realignment for nucleation. The latter is based on photochemical reaction by Xenon lamp illumination, in which the photoproducts can act as crystal nuclei as demonstrated by Okutsu and coauthors.[14] The advantages of laser induced crystallization are summarized into the following three points; (1) spatiotemporally controlled crystal nucleation and growth, (2) efficient and rapid nucleation from low supersaturated solution expecting high quality crystal, (3) controllable crystal morphology and polymorph by optimizing laser parameters such as intensity, wavelength, and polarization. However, the researchers of photophysical crystallization possibly face the difficulty that all of the techniques require pulsed laser from nanosecond to femtosecond duration or watts of continuous wave (CW) laser light to induce such photophysical phenomenon. For example, let us compare the required laser intensities for glycine crystallization. Since glycine is a typical molecule for a study of molecular crystallization mechanism, several groups have studied laser-induced crystallization of this compound. In the cases of nanosecond and femtosecond-pulsed laser-induced crystallization, laser peak power intensities of 2.4 GW/cm^2 (wavelength, 1064 nm; pulse duration, 9 ns)[2] and 63 TW/cm^2 (wavelength, 800 nm; pulse duration, 160 fs)[13] are employed to induce optical Kerr effect and transient pressure via optical breakdown of water, respectively. Sugiyama et al. have reported laser trapping-induced crystallization of glycine with 0.4 GW/cm^2 laser intensity (wavelength, 1064 nm, CW).[5] For further development of laser-induced crystallization, suppression of required laser energy is needed because of possible damage to molecule such as ionization and denaturation.

In this study, we propose a novel spatiotemporally controlled laser induced crystallization utilizing localized thermal microbubble. We have successfully obtained glycine crystals with continuous wave laser at several tens of mW equivalent to a few tens of MW/cm^2 laser intensity, which is much lower laser intensity compared to those used in the previous laser trapping crystallization. The mechanism is discussed in view of contributions of convection flow around the microbubble and rapid temperature jump at the bubble/water interface.

Glycine (99.0%, Wako Chemical) was used without further purification. We prepared glycine aqueous supersaturated solution at 3.6 M which is above saturation concentration

Received: December 19, 2011
Accepted: February 16, 2012
Published: February 16, 2012

(3.0 M). The solution was slowly heated up to 60 °C in water bath. The compaund was completely dissolved and then allowed to cool down to room temperature. A narrow line patterned gold nanoparticle thin film was prepared by vapor deposition on a quartz substrate[16,17] and the thickness was controlled by using quarts crystal microbalance (CRTM-7000, ULVAC). In this experiment, 20-nm thickness film was prepared and the thickness was confirmed by AFM measurement (See Supporting Information). The thin film substrate was sealed by a glass substrate with Parafilm™ spacers (about 40 μm thickness) as schematically shown in Figure 1 a. The

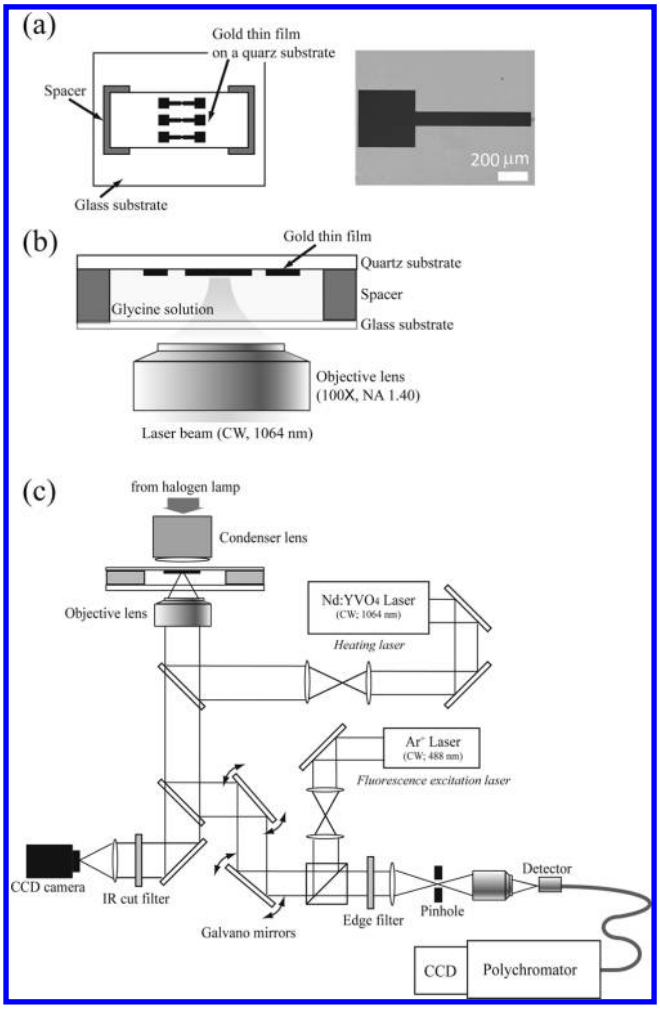

Figure 1. (a) Schematic illustration of a top view of a sample cell consisting from gold thin film on quartz substrate, glass substrate, and spacers. The right panel shows optical transmittance image of the gold thin film. (b) Side view of the sample cell with optical arrangement. (c) Schematic illustration of the total optical experimental setup.

glycine solution was supplied to the sample cell from the gap between glass and quartz substrates with capillarity and filled up the cell. The sample cell was put on an inverted microscope (IX-71, Olympus) coupled with a confocal unit (FV300, Olympus). To slow down solution evaporation, the sample was covered with a Petri dish. The gold film surface of the sample was exposed to CW near-infrared laser beam (J20-BL-106, Spectra Physics) through an oil immersion objective lens (100×, N.A. 1.40, UPlanApo, Olympus) as schematically illustrated in Figure 1 b. The laser power was varied in the range of 0−100 mW after the objective. Whole the experimental setup is shown in Figure 1 c. The crystallization process was observed with a digital CCD camera (CV−S3200N, JAI) attached to the microscope running at 30 interlaced frames per second. The reflection of the near-infrared laser beam was completely eliminated by a low pass filter placed in front of the CCD camera. Confocal fluorescence imaging and spectroscopy were carried out by excitation with 488 nm Ar^+ laser (20 mW, Melles Griot) irradiation through the identical objective lens to 1064 nm laser irradiation and fluorescence signal was recorded by both a pinphotodiode in the confocal unit for imaging and a CCD camera combined with polychromator (polychromator, SpectraPro 2300i; CCD camera, PIXIS400; Princeton Instruments) for spectroscopy after passing through a confocal aperture (500 μm). The spatial resolution of the confocal fluorescence microscope is 200 nm in lateral.

A representative time evolution of glycine crystal generation upon 1064 nm laser irradiation to gold thin film is shown in Figure 2. After a laser beam with 60 mW power was focused on the film surface (black area in Figure 2a), a single microbubble was observed at the focal point (Figure 2b) and gradually increased the size up to about 20 μm diameter (Figure 2 c) on the second time scale. The point where the bubble emerged was close proximity to the focal position of the laser irradiation. The bubble can be assumed to be a thermal microbubble as reported in previous literature.[16,17] Optical property of this gold film is different from that of the bulk gold because the film is consisted from gold nanoparticles. This localized plasmon resonance leads high absorption coefficient at 1064 nm, α = 1.65×10^7 (m^{-1}),[16] which can be assumed to result in local heating up to the boiling temperature of water. Once forming single bubble at the laser focus, it stably exists there without shrinkage and collapse. It can be considered that the bubble reaches the equilibrium state between heat transfer from the laser-heated substrate and heat dissipation to the surrounding medium. Note that lens effect of the bubble refracted the transmitted light and deformed the image of the corner of the gold thin film below the bubble (Figure 1c and see the Supporting Information, Figure S2). It should be mentioned that damage of the gold thin film surface was not induced when the bubble was stably kept at the focal point.

By varying the input laser power, we found that there was a threshold of the bubble formation around 15 mW. To estimate the temperature elevation at the focal point, we carried out a thermal diffusion calculation. When a Gaussian continuous wave laser beam is irradiated to highly absorption thin film surface, the temperature of the thin film surface, $T(r)$, as a function of the distance from the center of the focus, r, at steady-state is approximately described as eq 1.[18]

$$T(r) = T_0 + \frac{P(1-R)}{2\sqrt{\pi}\kappa\omega_0}(0.53 + 0.165\ln \alpha h) e^{-r^2/\omega_0^2} I_0\left(\frac{r^2}{2\omega_0^2}\right) \quad (1)$$

where $I_0(r)$ is the zero-th order modified Bessel function, with $I_0(0) = 1$. It is important to note that the equation is based on no heat loss and finite absorption of light ($0.1 < \alpha h < 10$; h, thickness of the film). Since the thermal diffusivity of a gold thin film is reported as 0.55×10^{-4} (m^2/s) at 25 nm thickness on a quartz substrate,[19] it is expected to reach steady-state in nano to microsecond order after laser irradiation.[18] T_0, κ, and R

dx.doi.org/10.1021/am201799b | ACS Appl. Mater. Interfaces 2012, 4, 1158−1163

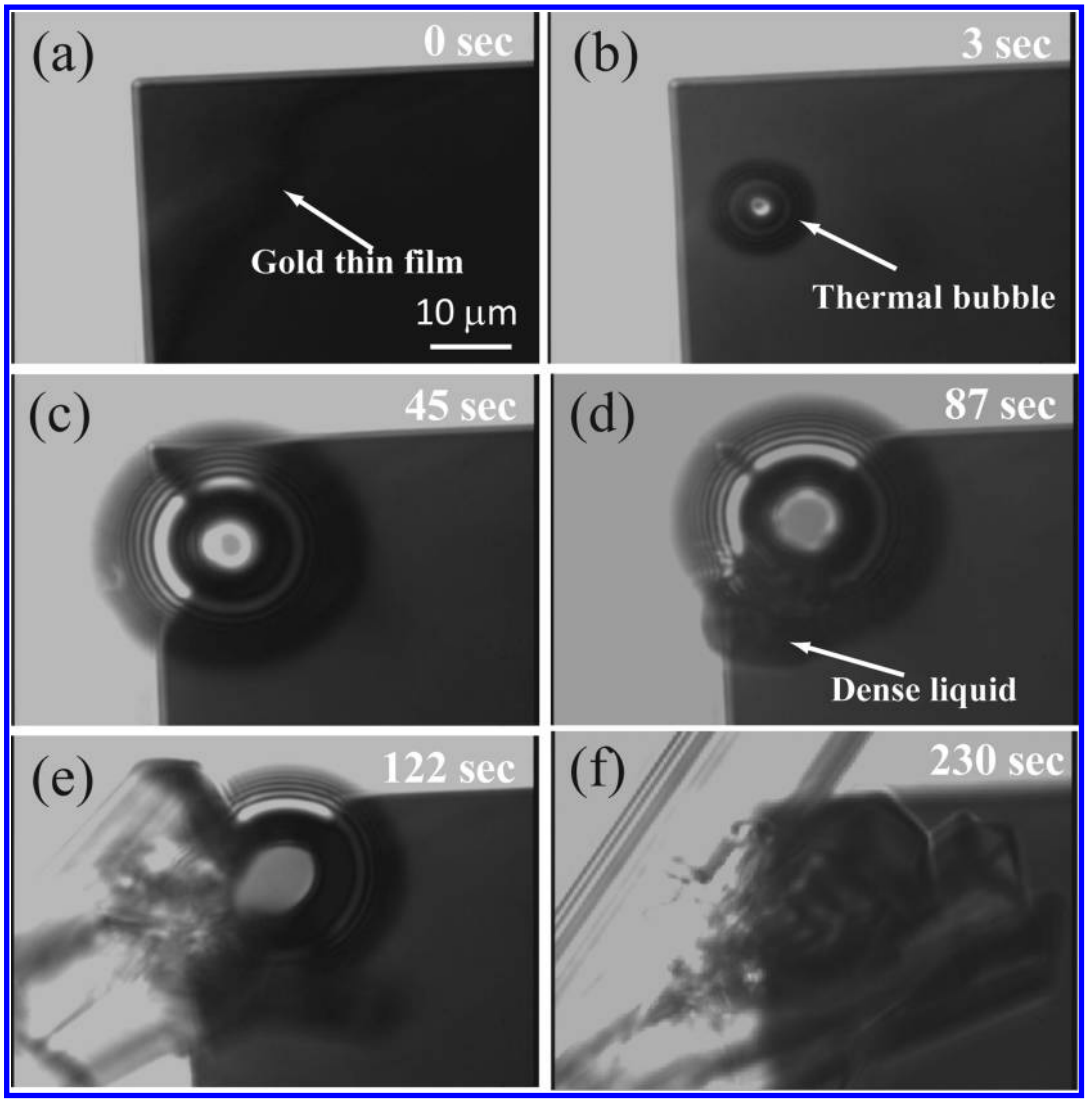

Figure 2. Representative time evolution of glycine crystal generation upon 60 mW CW 1064 nm laser irradiation to gold thin film.

are initial temperature, heat conductivity of medium and reflectivity coefficient of the film, respectively. P and ω_0 denote an incident laser power and the beam radius, respectively. Considering experimental conditions, the value of T_0, ω_0 was determined to be 293 (K) and 230 (nm), respectively. α, R, and κ of the gold film are set to 1.65×10^7 (m^{-1}), 0.25, and 38.5 (W/(m K)) from the literature, respectively.[16,20] Calculated temperature distribution on the gold film surface as a function of incident laser power P is shown in Figure 3. This calculation indicates that the experimentally obtained threshold of the bubble roughly agrees with the estimated laser power to reach a temperature at the focus spot on gold thin film surface to boiling point of water (373 K). In addition, above 80 mW irradiation, we confirmed that the laser beam formed a hole on the gold film at the focal point, this can also be explained from the calculation because the film temperature reaches its melting point (1337 K). Therefore, we can safely conclude that the bubble is assigned to a vapor bubble induced by laser heating.

After a certain time from the bubble generation (~1 min), fluctuating and transparent liquid domain was found around the bubble surface (Figure 2d). Because the liquid domain shows a clear boundary, the domain is not explained in terms of temperature fluctuation near the bubble. During laser irradiation, this domain could ensure its stability, while its shape was fluctuating. By replacing glycine solution to pure water, we confirmed that we could not observe the fluctuating liquid domain. This indicates that the liquid domain can be

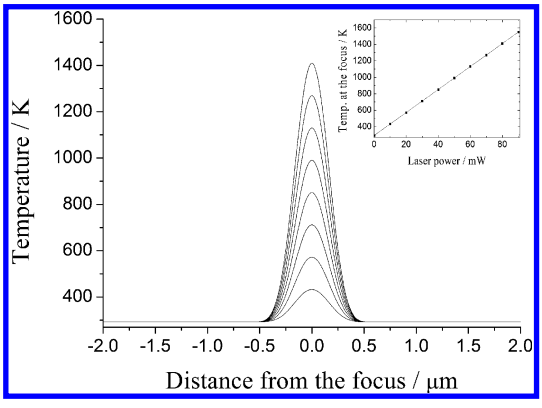

Figure 3. Calculated temperature profile at the gold thin film surface upon tightly focused laser beam irradiation to the film surface. The input power varies from 10 to 80 mW with 10 mW step. The inset shows the temperature at the center of the focus as a function of the input power.

dx.doi.org/10.1021/am201799b | ACS Appl. Mater. Interfaces 2012, 4, 1158–1163

ascribed to high concentration of glycine triggered by the bubble formation. Accordingly, the relatively high refractive index of the domain compared to bulk glycine solution and the indeterminate shape of the domain probably result in light refraction, elastic light scattering, or internal reflection, and thus the domain can be observed eventually. When we cut off the laser light after observing the liquid domain, crystal formation was initiated from the inside of the domain toward the outside (Figure 2e). The crystal growth spontaneously continued larger than several hundred micrometers size region (Figure 2f), and the growth speed was mainly affected by glycine concentration. The higher concentration tends to enhance faster crystal growth. It is obvious that single or multiple crystal(s), whose size finally reaches larger than several hundreds micrometer, is formed upon laser irradiation. On the other hand, the bubble remained for few tens seconds during the crystal growth, and shrinked gradually, and eventually disappeared (Figure 2f and see the Supporting Information, Figure S2). The reason of the long-lasting bubble without heat source remains unclear, but this is not found without crystallization or in the absence of glycine in solution. We assume that the highly dense glycine around the bubble can suppress heat dissipation from the bubble to the surrounding because of relatively lower thermal conductivity of glycine compared to water.[21] Furthermore, there is a possibility that glycine molecules were adsorbed on the bubble surface and act as a surfactant. Consequently, we succeeded in spatially controlled glycine nucleation and growth induced by the vapor microbubble formation. It should be noted that the threshold of required laser power for crystal generation was identical to that of thermal microbubble formation, around 15 mW as described above. The bubble size is strongly dependent on the incident laser power, and it is revealed that the higher power irradiation tends to generate multiple crystals in single sequence. Another example of crystallization process is represented in the Supporting Information.

It is important to note that we could not achieve the crystallization when the fluctuating liquid domain was not observed around the bubble in advance. Thus, the generation of the dense liquid domain around the bubble can be considered as a precursor of crystal, which is composed of highly dense liquid concentrate of glycine. Recently, our group found similar droplet formation of glycine despite that it was created by means of photon pressure induced molecular migration and accumulation at laser focal point.[22] Theoretically, the dense droplet can be explained in terms of metastable state of glycine realized by liquid–liquid phase separation via binodal decomposition.[23] Therefore, we suppose that the thermal microbubble generation may trigger not only molecular migration but also molecular accumulation toward the bubble interface, which leads to the fluctuating liquid domain formation as a precursor of crystal. This is supported by the fact that we have previously succeeded in accumulation of quantum dots around the bubble/water interface.[17]

To examine the above explanation, we replaced the glycine solution in the sample cell with 1 mM Rhodamine 6G (Sigma Aldrich) in water and generated the thermal microbubble in the same manner. As a result, at the place where the bubble formed, we found a circular fluorescent ring structure by confocal fluorescence microscope measurement (Figure 4). The diameter of the inner circle, which roughly corresponds to the contact size of the thermal microbubble (~5 μm), increased with input laser power, similarly to the character of quantum

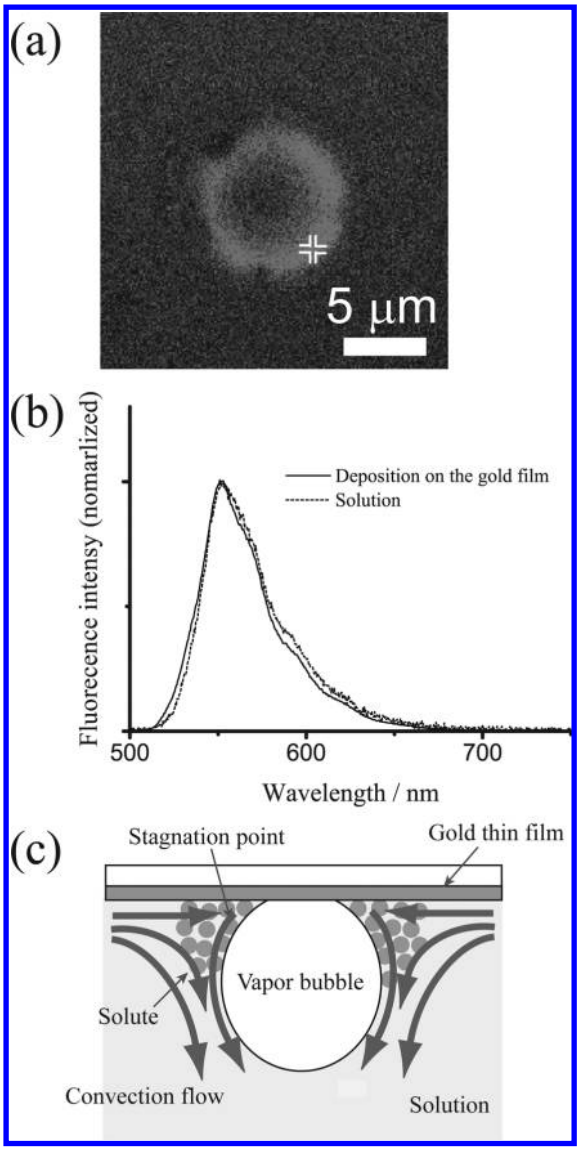

Figure 4. (a) Confocal fluorescence image and (b) spectrum of Rhodamine 6G transferred and deposited on a gold thin film by the thermal microbubble triggered convection flow. The spectrum was taken from the indicated position in image a. Fluorescence spectrum of Rhodamine 6G solution obtained by the same experimental setup is also shown in (b as a dotted line. Laser power for the microbubble formation was set to 30 mW. (c) Schematic illustration of convection flow induced by the vapor microbubble, which leads liquid–liquid phase separation of glycine at the bubble interface.

dots ring formation reported in the previous literature.[17] The fluorescence spectral shape of the ring structure (Figure 4b) can be assined to that of Rhodamine 6G, indicating the deposition clearly.. The small spectral change compared to that in solution suggests that the dye is molecularly deposited, not forming its aggregate appreciably. The molecular dispersion and aggregation condition of Rhodamine 6G on the film will be studied in more details in near future. The mechanism of Rhodamine 6G deposition upon the thermal bubble generation is explained as follows: Laser-heating of the gold thin film followed by water evaporation at the focal point causes temperature gradient from the bubble to the surrounding and induces thermal convection flow in opposite direction.[24] At the same time, temperature gradient induces surface tension

dx.doi.org/10.1021/am201799b | ACS Appl. Mater. Interfaces 2012, 4, 1158–1163

gradient, from contact point between the bubble and the gold film (low surface tension) to the top of the bubble (high) along the bubble surface, generating a Marangoni convection flow away from low to high surface tension area. Subsequently, liquid flow toward the contact point between the bubble and the film along the film surface is also induced, and it turns back at the contact point and converges with the Marangoni flow along the bubble surface. Thus, both thermal convection and Marangoni convection flows can transfer molecules toward the bubble surface. Importantly, a stagnation point of molecules should exist close to the gold/bubble/solution interface, because evaporating water is continuously replenished by surrounding solution.[25,26] Consequently, it can be considered that Rhodamine 6G molecules transferred by the convection flow were highly concentrated at the point and the ring structure of Rhodamine 6G was formed probably due to electrostatic adsorption on the gold film surface as shown in Figure 4a. In the case of glycine, along elevating temperature at the bubble/water interface, solubility of glycine should increase simultaneously according to the solubility curve, namely, solubility of molecules as a function of temperature.[27] Thus, higher concentration area of glycine can be realized at the bubble surface compared to bulk solution, so that we can safely conclude that the convection flow generated around the bubble initiates molecular migration to the bubble/solution/substrate interface and small molecules are able to be accumulated there, leading to liquid−liquid phase separation between glycine concentrate and water as schematically illustrated in Figure 4c.

Next, the trigger to nucleation from the high concentration area of glycine is considered. When we consider phase diagram, there is an energy barrier between the dense droplet and crystal, so that it should be overcome to generate a crystal.[23] In this viewpoint, cutting the laser light should play an important role which is schematically summarized in Figure 5. During the bubble generation at gold thin film, high density liquid concentrate of glycine can be obtained as explained above. When we cut off the laser light immediately, temperature is rapidly dropped down leading to the decrease in the solubility. The time required for heat dissipation from the laser focus is roughly expressed as $\omega_0/4D$,[18] where ω_0 and D denote beam radius and thermal diffusivity of gold thin film, respectively. With the values given above, the estimated time for heat dissipation is nanosecond order, which is faster than that of molecular diffusion to escape from the bubble surface. As the result, local molecular density is still higher at the bubble/water interface while the solubility decreases. Such rapid local temperature jump causing increase of local saturation degree may result in the density fluctuation of glycine that can reduce the free energy barrier for crystal nucleation as ten Wolde predicted.[28] Therefore, we consider the phase transition is realized at the bubble/water interface beyond the critical liquid-crystal phase transition energy barrier. Moreover, there is a possibility that the bubble/water interface can enhance molecular alignment due to the surface tension of bubble, possibly assisting nucleation. We propose to clarify our results by comparison of the present result with other molecules such as urea or other kinds of amino acid showing different solubility curves.

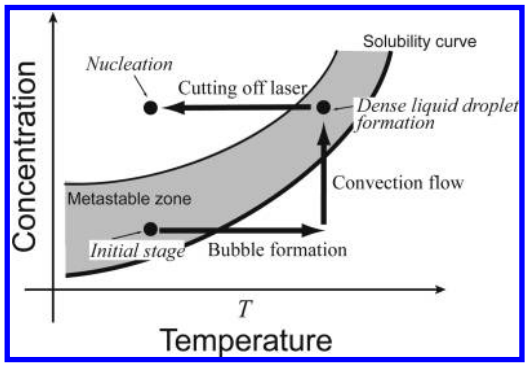

Figure 5. Possible scheme explaining the glycine crystallization at the microbubble/water interface based on the phase diagram.

In conclusion, we have demonstrated glycine crystallization utilizing thermal microbubble. By focusing CW near-infrared laser irradiation on a gold nanoparticle film, a single thermal microbubble is generated at the focal point. The temperature gradient around the bubble and along the bubble surface can provide a thermal and Marangoni convection flows to the focal point, respectively, initiating nucleation by way of dense liquid domain formation at the interface. Importantly, required laser power for the crystal formation is much lower than the other laser induced crystallization method, down to several tens mW with a high numerical aperture objective (few tens of MW/cm^2 order). This spatiotemporally controlled crystallization technique possesses high potential in crystal patterining. As the next step, other kinds of organic molecules including proteins will be investigated. Moreover, the current gold nanoparticle film can be replaced with individual gold nanoparticles as a local heat source, which is expected to suppress heat damage from the substrate.

■ ASSOCIATED CONTENT

Supporting Information

Height profile of the gold thin film measured by AFM, four examples of the glycine crystallization process upon laser irradiation on gold thin film surface, and Raman spectrum of the obtained crystal. This material is available free of charge via the Internet at http://pubs.acs.org.

■ AUTHOR INFORMATION

Corresponding Author

*E-mail: uwada@mail.nctu.edu.tw (T.U.); masuhara@masuhara.jp (H.M.).

Notes

The authors declare no competing financial interest.

■ ACKNOWLEDGMENTS

The present work was partially supported by the MOE-ATU Project (National Chiao Tung University) from the Ministry of Education of Taiwan, the National Science Council of Taiwan to T.U. (NSC 98-2113-M-009-013-MY2), T.S. (NSC 100-2113-M-492-002-MY2), and to H.M. (NSC 98-211-M-009-001). We also thank to KAKENHI grant (a Grant-in-Aid for Scientific Research) in the Priority Area "Molecular Science for Supra Functional Systems" (19056009) to T.U., a KAKENHI (S) grant (18106002) to H.M., and JSPS fellowship to S.F. from the Japan Society for the Promotion of Science (JSPS) and Chuo University Joint Research Grant 2009 from Chuo University to M.H.

REFERENCES

(1) Zaccaro, J.; Matic, J.; Myerson, A. S.; Garetz, B. A. *Cryst. Growth Des.* **2001**, *1*, 5.
(2) Sun, X.; Garetz, B. A.; Myerson, A. S. *Cryst. Growth Des.* **2006**, *6*, 684.
(3) Alexander, A. J.; Camp, P. J. *Cryst. Growth Des.* **2008**, *9*, 958.
(4) Duffus, C.; Camp, P. J.; Alexander, A. J. *J. Am. Chem. Soc.* **2009**, *131*, 11676.
(5) Sugiyama, T.; Adachi, T.; Masuhara, H. *Chem. Lett.* **2007**, *36*, 1480.
(6) Tsuboi, Y.; Shoji, T.; Kitamura, N. *Jpn. J. Appl. Phys.* **2007**, *46*, L1234.
(7) Rungsimanon, T.; Yuyama, K.; Sugiyama, T.; Masuhara, H.; Tohnai, N.; Miyata, M. *J. Phys. Chem. Lett.* **2010**, *1*, 599.
(8) Rungsimanon, T.; Yuyama, K.; Sugiyama, T.; Masuhara, H. *Cryst. Growth Des.* **2010**, *10*, 4686.
(9) Adachi, H.; Takano, K.; Hosokawa, Y.; Inoue, T.; Mori, Y.; Matsumura, H.; Yoshimura, M.; Tsunaka, Y.; Morikawa, M.; Kanaya, S.; Masuhara, H.; Kai, Y.; Sasaki, T. *Jpn. J. Appl. Phys.* **2003**, *42*, L798.
(10) Lindinger, B.; Mettin, R.; Chow, R.; Lauterborn, W. *Phys. Rev. Lett.* **2007**, *99*, 045701.
(11) Murai, R.; Yoshikawa, H. Y.; Takahashi, Y.; Maruyama, M.; Sugiyama, S.; Sazaki, G.; Adachi, H.; Takano, K.; Matsumura, H.; Murakami, S.; Inoue, T.; Mori, Y. *Appl. Phys. Lett.* **2010**, *96*, 043702.
(12) Soare, A.; Dijkink, R.; Pascual, M. R.; Sun, C.; Cains, P. W.; Lohse, D.; Stankiewicz, A. I.; Kramer, H. J. M. *Cryst. Growth Des.* **2011**, *11*, 2311.
(13) Uwada, T.; Liu, T.-H.; Sugiyama, T.; Usman, A.; Hosokawa, Y.; Masuhara, H. *J. Cryst. Growth* **2012**, submitted.
(14) Furuta, K.; Horiuchi, H.; Hiratsuka, H.; Okutsu, T. *Cryst. Growth Des.* **2008**, *8*, 1886.
(15) Ward, M. R.; Copeland, G. W.; Alexander, A. J. *J. Chem. Phys.* **2011**, *135*, 114508.
(16) Fujii, S.; Kobayashi, K.; Kanaizuka, K.; Okamoto, T.; Toyabe, S.; Muneyuki, E.; Haga, M. *Chem. Lett.* **2009**, *39*, 92.
(17) Fujii, S.; Kanaizuka, K.; Toyabe, S.; Kobayashi, K.; Muneyuki, E.; Haga, M. *Langmuir* **2011**, *27*, 8605.
(18) Bäuerle, D. *Laser Processing and Chemistry*, fourth ed.; Springer: New York, 1996.
(19) Takata, Y.; Haneda, H.; Mitsuhashi, T.; Wada, Y. *Appl. Surf. Sci.* **2002**, *189*, 227.
(20) Chen, G. *Appl. Phys. Lett.* **1999**, *74*, 2942.
(21) Simmons, J. A. *Nature* **1967**, *216*, 1302.
(22) Yuyama, K.; Sugiyama, T.; Masuhara, H. *J. Phys. Chem. Lett.* **2010**, *1*, 1321.
(23) Vekilov, P. G. *Cryst. Growth Des.* **2004**, *4*, 671.
(24) Braun, D.; Libchaber, A. *Phys. Rev. Lett.* **2002**, *89*, 188103.
(25) Xu, X.; Luo, J. *Appl. Phys. Lett.* **2007**, *91*, 124102.
(26) Deegan, R. D.; Bakajin, O.; Dupont, T. F.; Huber, G.; Nagel, S. R.; Witten, T. A. *Nature* **1997**, *389*, 827.
(27) Kunihisa, K. S. *J. Cryst. Growth* **1974**, *23*, 351.
(28) ten Wolde, P. R.; Frenkel, D. *Science* **1997**, *277*, 1975.